

PHYSICAL METHODS
OF INVESTIGATION

Structure and Luminescent Properties of Solid Solutions

$\text{Sm}_{2-x}\text{Eu}_x(\text{MoO}_4)_3$

M. V. Raskina, V. A. Morozov, A. V. Pavlenko, I. G. Samatov,
I. V. Arkhangel'skii, S. Yu. Stefanovich, and B. I. Lazoryak

Moscow State University, Moscow, 119991 Russia

E-mail: masha.raskina@gmail.com

Received July 4, 2014

Abstract—Solid solutions $\text{Sm}_{2-x}\text{Eu}_x(\text{MoO}_4)_3$ ($0 \leq x \leq 2$) have been prepared as two modifications: monoclinic α modification with a distorted scheelite structure and orthorhombic β' modification with a non-scheelite structure. The $\alpha \rightarrow \beta'$ phase transition is accompanied by a considerable increase in the unit cell volume ($\sim 24\%$). For all solid solutions, the strongest transition is ${}^5D_0 \rightarrow {}^7F_2$ of Eu^{3+} cations responsible for the red luminescence of the samples ($\lambda_{\text{max}} \sim 616$ nm). Whatever the type of $\text{Sm}_{2-x}\text{Eu}_x(\text{MoO}_4)_3$ structure, the luminescence maximum is in the concentration range $1.75 < x \leq 2$; for the α - and β' -modifications, different luminescence excitation mechanisms have been found.

DOI: 10.1134/S0036023615010118

In recent years, molybdates and tungstates of different composition are being increasingly used in modern technology due to the possibility of varying their physicochemical, electrophysical, and optical characteristics in a wide range of compositions. Among them are found phosphors, laser materials, piezoelectrics, and ferroelectrics [1]. Particular attention is given to molybdates and tungstates containing luminescent elements (Ce, Pr, Eu, Tb, Tm), which can be used as a phosphor for white light-emitting diodes (WLED) [2, 3].

One of the most common ways of generating white light in modern WLEDs is mixing light from red, blue, and green phosphors. However, the luminescence intensity of the red phosphor ($\text{Y}_2\text{O}_2\text{S}:\text{Eu}^{3+}$), most frequently used in the LED industry, is eight times lower than that of the corresponding green ($\text{ZnS}:(\text{Cu}^+, \text{Al}^{3+})$) and blue ($\text{BaMgAl}_{10}\text{O}_{17}:\text{Eu}^{2+}$) phosphors [2, 4]. Increasing the luminescence intensity of a phosphor emitting in the red region of the visible light (625–740 nm), will significantly increase the light output of WLEDs in general. Candidate materials that can replace $\text{Y}_2\text{O}_2\text{S}:\text{Eu}^{3+}$ in WLEDs are materials also containing Eu^{3+} cations, since the maximum luminescence intensity for Eu^{3+} cation is observed for the ${}^5D_0 \rightarrow {}^7F_2$ transition at ~ 613 – 616 nm [2, 5–11]. Another reason to use Eu^{3+} -containing compounds in design of red phosphors for WLEDs is the fact that the luminescence excitation energy of the Eu^{3+} cations matches with the energy emitted by the semiconductor of an LED ($\lambda = 270$ – 400 nm) [2–5]

Compounds $\text{R}_2(\text{MoO}_4)_3$ (R is a rare earth element) containing Eu^{3+} cations are promising materials for red phosphors since for some of these compounds, for

example, β' - $\text{Gd}_2(\text{MoO}_4)_3:0.4\text{Eu}^{3+}$, the luminescence intensity in the range ~ 615 – 616 nm is comparable to the luminescence intensity of $\text{Y}_2\text{O}_2\text{S}:\text{Eu}^{3+}$ [12]. The $\text{R}_2(\text{MoO}_4)_3$ compounds are easy to synthesize, thermally stable, and, unlike $\text{Y}_2\text{O}_2\text{S}:\text{Eu}^{3+}$, is not degraded by sunlight [13]. It should also be noted that the luminescence excitation spectra of these compounds show a broad, strong absorption band in the range 200–350 nm characterizing the charge transfer from O^{2-} in MoO_4^{2-} groups through the Mo–O bonds to the luminescent centers [2, 3, 6–10, 14]. Thus, the strong luminescence of $\text{R}_2(\text{MoO}_4)_3:\text{L}$ compounds (L is a luminescent element) can be caused not only by the use of the energy required for the direct excitation of luminescent centers ($\lambda_{\text{ex}} \sim 299$ nm for Tb^{3+} [15], ~ 352 nm for Dy^{3+} [16], ~ 379 nm for the Er^{3+} [17], ~ 395 nm for Eu^{3+} [2], etc.), but also with the use of radiation at shorter wavelengths (260–280 nm). For example, it has been demonstrated [14] that, $\lambda_{\text{ex}} = 280$ nm, the luminescence intensity of α - $\text{Gd}_{1.25}\text{Eu}_{0.75}(\text{MoO}_4)_3$ in the range of the ${}^5D_0 \rightarrow {}^7F_2$ transition of Eu^{3+} cations ($\lambda_{\text{max}} \sim 616$ nm) is ~ 1.5 times higher than at $\lambda_{\text{ex}} = 395$ nm. Accordingly, the possibility of manifestation of additional contributions to the luminescence excitation mechanism for increasing its intensity allow one to treat $\text{R}_2(\text{MoO}_4)_3$ compounds as promising “guest” structures for doping or substitution of R^{3+} cations by other lanthanides and thereby to create new phosphors systems.

Structural diversity of triple molybdates $\text{R}_2(\text{MoO}_4)_3$ was considered for the first time in [18]. Later, the structural data for various modifications have been

refined and it has been demonstrated that the stability of different crystalline modifications depends not only on the lanthanide but also on the conditions of preparing these compounds. In general, the structures of $R_2(\text{MoO}_4)_3$ compounds can be divided into two types: scheelite-like (based on the structure of natural mineral scheelite CaWO_4) and non-scheelite (Fig. 1). For scheelite structures $R_2\Box(\text{MoO}_4)_3$ (\Box is a cation vacancy), four variants of crystallization are known: (1) tetragonal (space group $I4_1/a$) [19, 20] with a random distribution of cations and vacancies over the positions of the structure; (2) monoclinic (space group $C2/c$) with a $\text{La}_2(\text{MoO}_4)_3$ structure with the ordering of vacancies in the cation sublattice along the (100) direction [21]; (3) monoclinic (space group $C2/c$) with a $\text{Eu}_2(\text{WO}_4)_3$ structure (structure of commonly referred to as α modification) with the ordering of vacancies in the cation sublattice along the (110) direction [22–24]; (4) monoclinic with an incommensurate modulated structure of $\text{Pr}_2(\text{MoO}_4)_3$ (space group $I2/b(\alpha\beta)00$) [25]. For non-scheelite structures of $R_2\Box(\text{MoO}_4)_3$ compounds, three variants are known: (1) orthorhombic β' phase with ferroelectric-ferroelastic properties (space group $Pba2$) [26, 27]; (2) tetragonal β phase with paraelectric-paraelastic properties (space group $P\bar{4}2_1m$) [27]; (3) orthorhombic (space group $Pbcn$) with a $\text{Sc}_2(\text{WO}_4)_3$ structure [28, 29].

The effect of substitution of Eu^{3+} for Sm^{3+} cations in $\text{Sm}_{2-x}\text{Eu}_x(\text{MoO}_4)_3$ solid solutions on the luminescent properties has not been studied so far. Nevertheless, a similar study of the $\text{Gd}_{2-x-y}\text{Eu}_x\text{Sm}_y(\text{MoO}_4)_3$ solid solutions ($0 \leq x \leq 2$, $0 \leq y \leq 0.04$) [30] has shown that the substitution of Sm^{3+} cations for Gd^{3+} cations leads to a significant increase in luminescence intensity. For example, the luminescence intensity of the ${}^5D_0 \rightarrow {}^7F_2$ transition for $\alpha\text{-Gd}_{0.776}\text{Eu}_{1.2}\text{Sm}_{0.024}(\text{MoO}_4)_3$ and $\beta'\text{-Gd}_{0.372}\text{Eu}_{1.6}\text{Sm}_{0.028}(\text{MoO}_4)_3$ is significantly higher than that for $\alpha\text{-Gd}_{0.8}\text{Eu}_{1.2}(\text{MoO}_4)_3$ and $\beta'\text{-Gd}_{0.4}\text{Eu}_{1.6}(\text{MoO}_4)_3$, respectively. The luminescence intensities of the ${}^5D_0 \rightarrow {}^7F_2$ transition for $\beta'\text{-Gd}_{0.372}\text{Eu}_{1.6}\text{Sm}_{0.028}(\text{MoO}_4)_3$ and the standard red phosphor $\text{Y}_2\text{O}_2\text{S}:\text{Eu}^{3+}$ are almost the same.

The aim of this study is to study the influence of the structure and Eu^{3+} concentration on the luminescent properties of $\text{Sm}_{2-x}\text{Eu}_x(\text{MoO}_4)_3$ solid solutions, crystallizing in two modifications: monoclinic α phases with a distorted scheelite structure and β' phases with a non-scheelite structure.

EXPERIMENTAL

Monoclinic solid solutions $\alpha\text{-Sm}_{2-x}\text{Eu}_x(\text{MoO}_4)_3$ were synthesized by a ceramic method from stoichiometric amounts of MoO_3 , Eu_2O_3 , and Sm_2O_3 (all oxides of chemically pure grade). Mixtures were annealed in two steps: at 823 K for 10 h and at 1023 K for 48 h with intermittent grinding. Orthorhombic solid solutions $\beta'\text{-Sm}_{2-x}\text{Eu}_x(\text{MoO}_4)_3$ ($0 \leq x \leq 2$) were obtained from the

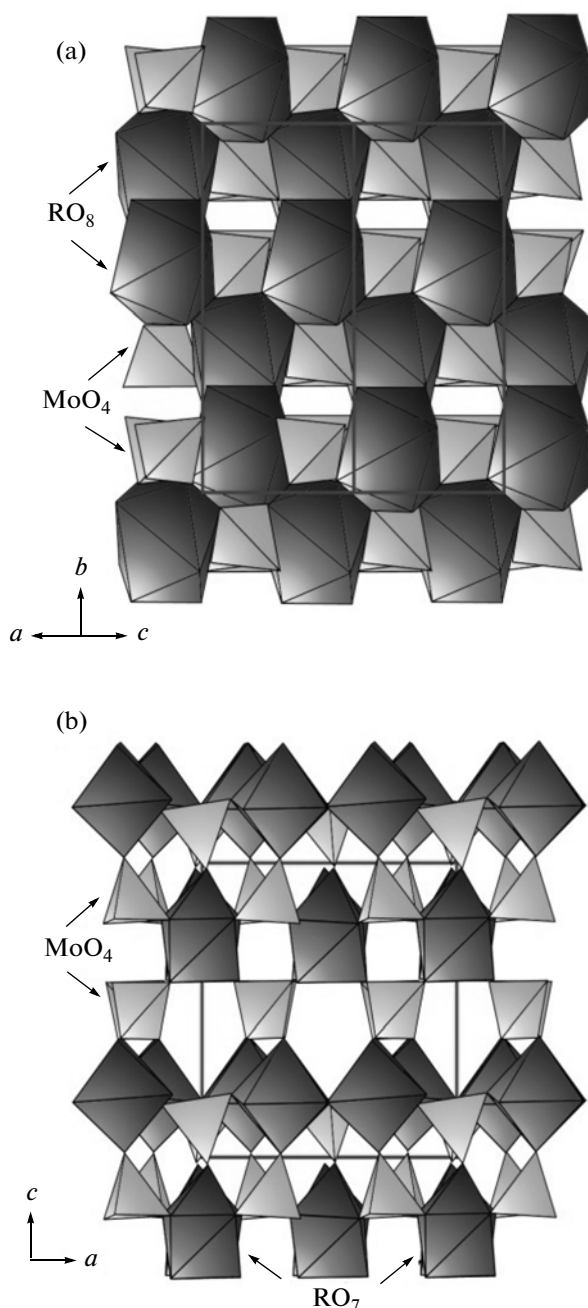


Fig. 1. RO_n polyhedra and MoO_4 tetrahedral in (a) monoclinic $\alpha\text{-R}_2(\text{MoO}_4)_3$ (space group $C2/c$) and (b) orthorhombic ($\beta'\text{-R}_2(\text{MoO}_4)_3$) (space group $Pba2$) structures.

corresponding monoclinic $\alpha\text{-Sm}_{2-x}\text{Eu}_x(\text{MoO}_4)_3$ by annealing at 1293 K for 24 h and subsequent quenching from this temperature in air.

X-ray powder diffraction analysis (XRD) of polycrystalline $\text{Sm}_{2-x}\text{Eu}_x(\text{MoO}_4)_3$ samples ($0 \leq x \leq 2$) was performed on the basis of experimental data obtained at room temperature on a Huber G670 Guinier diffractometer ($\text{CuK}\alpha_1$ radiation, $\lambda = 0.154056 \text{ \AA}$, transmission geometry, curved $\text{Ge}(111)$ monochromator,

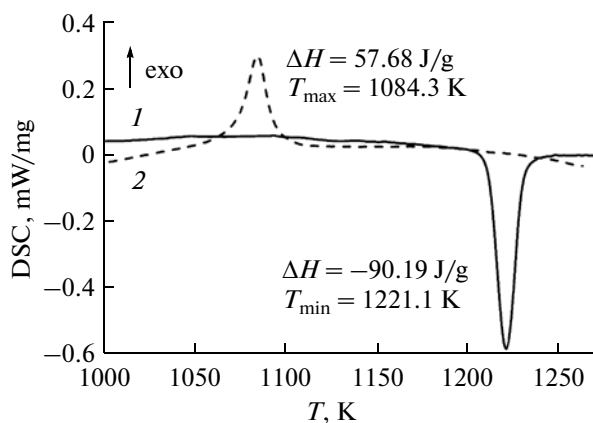


Fig. 2. Fragments of DSC curves for $\text{Sm}_2(\text{MoO}_4)_3$ in a successive cycle: (1) heating and (2) cooling.

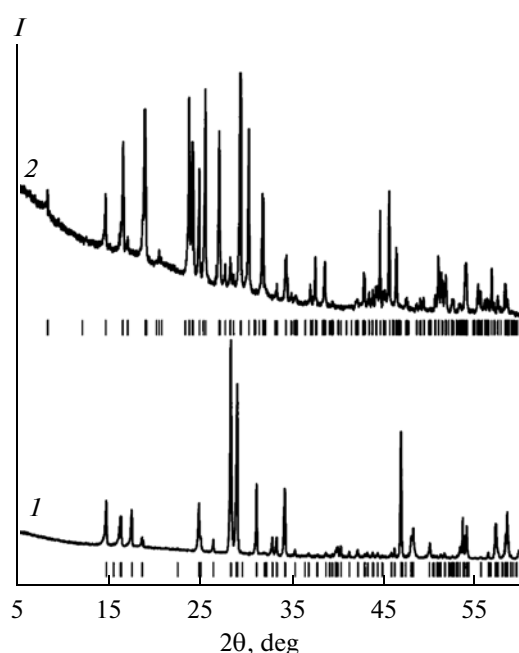


Fig. 3. Fragments of X-ray powder diffraction patterns of (1) α - and (2) β' - $\text{Sm}_2(\text{MoO}_4)_3$ (the ticks show the Bragg reflection positions for the monoclinic α - (space group $C2/c$) and orthorhombic (space group $Pba2$) β' phases).

2θ range is 4° – 100° with a step of 0.01°). Unit cell parameters of $\text{Sm}_{2-x}\text{Eu}_x(\text{MoO}_4)_3$ solid solutions were refined using Le Bail refinement in the JANA2006 software.

Study of $\text{Sm}_2(\text{MoO}_4)_3$ differential scanning calorimetry (DSC) and thermogravimetry (TG) was carried out on a NETZSCH STA Jupiter 409N simultaneous thermal analyzer at 313–1273 and 1273–973 K (heating/cooling at a rate of 5 K/min) in an argon atmosphere. The sample weight was ~ 50 mg. Samples were placed into platinum crucibles with lids. The relative

error of weight change determination was $\Delta = 1\%$, and that of heat effects was $\Delta = 2$ – 5% .

The luminescent properties of $\text{Sm}_{2-x}\text{Eu}_x(\text{MoO}_4)_3$ were studied on a Perkin Elmer LS 55 single-beam luminescence spectrophotometer. A 150-W pulsed xenon lamp was used as a source of excitation. The luminescence excitation spectra were recorded in the range 200–550 nm ($\lambda_{\text{em}} = 616$ nm). The luminescence spectra were measured at room temperature in the range 550–750 nm at the excitation wavelength $\lambda_{\text{ex}} = 395$ and 270 nm (for β' - $\text{Sm}_{2-x}\text{Eu}_x(\text{MoO}_4)_3$). A Hamamatsu R928 photomultiplier was used as a detector, and polycrystalline α - $\text{Eu}_2(\text{MoO}_4)_3$ was used as a reference. The luminescence intensity maximum of α - $\text{Eu}_2(\text{MoO}_4)_3$ was taken as 100%, and the luminescence intensities of the other samples were normalized to the former.

Optical second harmonic generation (SHG) in α - and β' - $\text{R}_2(\text{MoO}_4)_3$ ($R = \text{Eu}, \text{Sm}$) was measured using an YAG:Nd laser ($\lambda_{\text{w}} = 1064$ nm). The incident laser beam was perpendicular to the flat surface of a powder sample. Scattered radiation at the second-harmonic wavelength $\lambda_{2\omega} = 0.532$ nm was focused on the photomultiplier window, and its electric response was measured with a pulsed voltmeter and normalized to the $I_{2\omega}(\text{SiO}_2)$ signal of a reference quartz sample—a fine crystalline α -quartz powder with a particle size of 3–5 μm .

RESULTS AND DISCUSSION

Figure 2 shows fragments of the DSC curves for $\text{Sm}_2(\text{MoO}_4)_3$ in a heating–cooling cycle. The heating curve shows the only minimum at 1221 K, which is evidence of the endothermic first-order phase transition in $\text{Sm}_2(\text{MoO}_4)_3$ corresponding to the transition from the monoclinic α to the orthorhombic β' (tetragonal β) modification ($T_{\text{pt}} = 1212$ K). The cooling curve shows the only maximum characterizing the exothermic first-order phase transition from the β' (β) to the α modification ($T_{\text{pt}} = 1073$ K), which is evidence of reversibility of the $\alpha \leftrightarrow \beta'$ (β) phase transition. According to TG data, the $\text{Sm}_2(\text{MoO}_4)_3$ sample has no weight loss in the entire temperature range studied.

X-ray diffraction patterns of the α - and β' modifications are shown in Fig. 3. The results of refinement of the unit cell parameters for the monoclinic and orthorhombic $\text{Sm}_{2-x}\text{Eu}_x(\text{MoO}_4)_3$ modifications are presented in Tables 1 and 2, respectively. As follows from Tables 1 and 2, an increase in the Eu^{3+} content upon its substitution for Sm^{3+} cations in $\text{Sm}_{2-x}\text{Eu}_x(\text{MoO}_4)_3$ solid solutions ($0 \leq x \leq 2$) leads to a decrease in the unit cell parameters because of the smaller ionic radius of the Eu^{3+} cation ($r_{\text{VIII}} = 1.066$ Å [31]) as compared to Sm^{3+} ($r_{\text{VIII}} = 1.079$ Å [31]). It should be noted that, for all $\text{Sm}_{2-x}\text{Eu}_x(\text{MoO}_4)_3$ solid solutions, whatever the x value, the $\alpha \rightarrow \beta'$ phase tran-

Table 1. Results of refinement of unit cell parameters of α -Sm_{2-x}Eu_x(MoO₄)₃ ($0 \leq x \leq 2$) solid solutions ($0 \leq x \leq 2$) (space group *C2/c*, $Z = 4$) and literature data

x	$a, \text{\AA}$	$b, \text{\AA}$	$c, \text{\AA}$	β, deg	$V, \text{\AA}^3$	Reference
0	7.562	11.509	11.557	108.98	951.1	[22]
0	7.5535(4)	11.5021(7)	11.5675(7)	109.180(3)	949.21	[23]
0	7.5495(1)	11.5088(1)	11.5786(1)	109.126(1)	950.48(2)	This work
0.25	7.5487(1)	11.5045(1)	11.5725(1)	109.138(1)	949.46(3)	This work
0.5	7.5533(1)	11.4999(1)	11.5636(1)	109.170(1)	948.75(2)	This work
0.75	7.5510(1)	11.4934(1)	11.5554(1)	109.172(1)	947.24(2)	This work
1	7.5569(1)	11.4897(1)	11.5424(1)	109.228(1)	946.28(2)	This work
1.25	7.5550(1)	11.4844(1)	11.5368(1)	109.232(1)	945.12(2)	This work
1.5	7.5548(1)	11.4799(1)	11.5305(1)	109.244(1)	944.15(2)	This work
1.75	7.5537(1)	11.4739(1)	11.5225(1)	109.257(1)	942.78(2)	This work
2	7.5503(1)	11.4707(2)	11.5195(2)	109.259(1)	941.83(3)	This work
2	7.554	11.459	11.497	109.08	940.06	[22]
2	7.5463(3)	11.4529(6)	11.4974(6)	109.284(4)		[24]

Table 2. Results of refinement of unit cell parameters of β' -Sm_{2-x}Eu_x(MoO₄)₃ solid solutions ($0 \leq x \leq 2$) (space group *Pba2*, $Z = 4$) and literature data

x	$a, \text{\AA}$	$b, \text{\AA}$	$c, \text{\AA}$	$V, \text{\AA}^3$	Reference
0	10.4352	10.4718	10.7687	1176.76	[22]
0	10.4356(1)	10.4705(1)	10.76705(9)	1176.46(3)	This work
0.25	10.43181(9)	10.46635(9)	10.76186(8)	1175.01(2)	This work
0.5	10.43062(8)	10.46500(8)	10.75825(7)	1174.33(2)	This work
0.75	10.42447(8)	10.45985(8)	10.75297(7)	1172.49(2)	This work
1	10.4215(1)	10.4591(1)	10.74765(9)	1171.13(2)	This work
1.25	10.41817(8)	10.45227(8)	10.74314(7)	1169.86(2)	This work
1.5	10.41627(7)	10.45024(7)	10.73938(6)	1169.01(2)	This work
1.75	10.41302(7)	10.44675(7)	10.73245(6)	1167.50(2)	This work
2	10.41077(8)	10.44404(7)	10.72834(6)	1166.50(2)	This work
2	10.4109	10.4436	10.7269	1166.29	[22]

sition is accompanied by a considerable increase in the unit cell volume ($\sim 24\%$) (Fig. 4; Tables 1, 2).

The lack of a noticeable SHG signal (< 0.02) for the α -R₂(MoO₄)₃ samples (R = Eu, Sm) is evidence of the presence of the center of symmetry in the structure of these compounds and confirms the choice of the space group (*C2/c*). For analogous orthorhombic β' modifications, the SHG signal differed from zero and corresponded to $I_{2\omega}/I_{\omega}(\text{SiO}_2) \sim 53$ (Sm) and ~ 70 (Eu), which enables the conclusion that these structures have no center of symmetry. This is consistent with the choice of the polar space group *Pba2*.

The luminescence excitation spectra of α - and β' -Eu₂(MoO₄) recorded at $\lambda_{\text{em}} = 616$ nm (Fig. 5) show a broad strong absorption band in the range 200–350 nm and a set of peaks corresponding to intraconfiguration $4f^6-4f^6$ of Eu³⁺ cations in the range 350–550 nm. The strongest peaks correspond to the transitions ${}^7F_0 \rightarrow {}^5L_6$ (394–396 nm), ${}^7F_0 \rightarrow {}^5D_2$ (465–467 nm), and ${}^7F_0 \rightarrow {}^5D_1$ (537–539 nm). As shown in Fig. 5, for the monoclinic α -Eu₂(MoO₄) modification, the strongest luminescence excitation intensity is observed for the ${}^7F_0 \rightarrow {}^5L_6$ transition ($\lambda_{\text{max}} \sim 395$ nm), whereas for the orthorhombic β' modification, the luminescence intensity maximum corresponds to a broad absorption

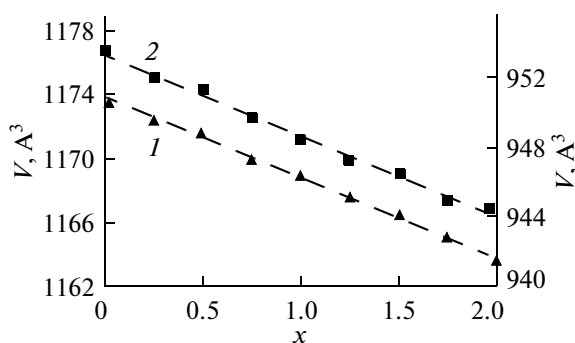


Fig. 4. Unit cell volume of (1) α - and (2) β' - $\text{Sm}_{2-x}\text{Eu}_x(\text{MoO}_4)_3$ vs. the Eu^{3+} content.

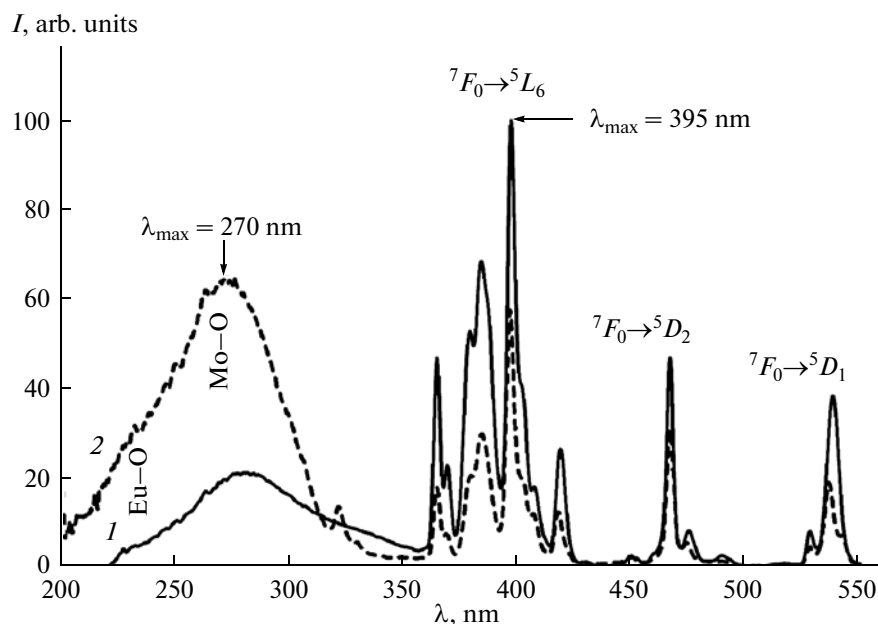


Fig. 5. Luminescence excitation spectra of (1) α - and (2) β' - $\text{Eu}_2(\text{MoO}_4)_3$, $\lambda_{\text{em}} = 616$ nm.

band with a maximum at $\lambda_{\text{max}} \sim 270$ nm. The intensity of this absorption band for the β' phase is three times higher than the intensity for the α phase.

In addition, for the orthorhombic β' phase, the above wide absorption band (in the range 200–350 nm) has two components with maxima at $\lambda_{\text{max}} \sim 240$ and ~ 270 nm. According to the literature data [2, 3, 6–10, 14, 32, 33], the first component ($\lambda_{\text{max}} \sim 240$ nm) corresponds to absorption bands that characterize charge transfer through the $\text{O}^{2-}-\text{Eu}^{3+}$ bonds, whereas the second component ($\lambda_{\text{max}} \sim 270$ nm) characterizes charge transfer from O^{2-} in MoO_4^{2-} groups to the luminescent centers through the Mo–O bonds. Thus, comparison of the luminescence excitation spectra enables the conclusion that there are two radically different luminescence excitation mechanisms, which have different contributions for α - and β' - $\text{Eu}_2(\text{MoO}_4)_3$: (1) direct excitation of luminescent centers (Eu^{3+} cations) and

(2) by means of charge transfer from O^{2-} in MoO_4^{2-} groups to luminescent centers through Mo–O bonds.

Analysis of luminescence spectra for α - and β' - $\text{Eu}_2(\text{MoO}_4)_3$ recorded at different excitation energies ($\lambda_{\text{ex}} = 395$ and 270 nm) demonstrates that the luminescence of $\text{Eu}_2(\text{MoO}_4)_3$ is associated with the $^5D_0 \rightarrow ^7F_j$ ($j = 0, 1, 2, 3, 4$) of Eu^{3+} cation, the largest intensity being inherent in the $^5D_0 \rightarrow ^7F_2$ transition responsible for the red luminescence of the samples ($\lambda_{\text{max}} \sim 616$ nm) (Fig. 6). Figures 7–9 show the luminescence spectra of α - and β' - $\text{Sm}_{2-x}\text{Eu}_x(\text{MoO}_4)_3$ ($0 \leq x \leq 2$) solid solutions and their luminescence intensity in the range of the $^5D_0 \rightarrow ^7F_2$ transition as a function of Eu^{3+} concentration. According to the data obtained, the increase in Eu^{3+} concentration upon the substitution of Eu^{3+} for Sm^{3+} cations in $\text{Sm}_{2-x}\text{Eu}_x(\text{MoO}_4)_3$ solid solutions leads to an increase in luminescence intensity in the range of the $^5D_0 \rightarrow ^7F_2$ transition. The luminescence intensity maximum, irrespective of the structure type, is observed in the concentration range $1.75 \leq x \leq 2$. The

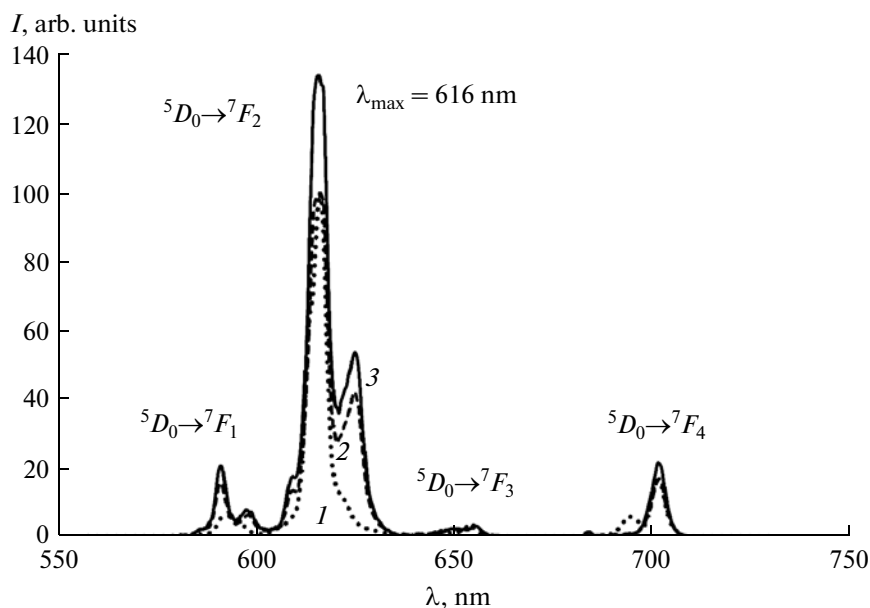


Fig. 6. Luminescence spectra of (1) α - $\text{Eu}_2(\text{MoO}_4)_3$ ($\lambda_{\text{ex}} = 395$ nm) and (2, 3) β' - $\text{Eu}_2(\text{MoO}_4)_3$ at $\lambda_{\text{ex}} =$ (2) 395 and (3) 270 nm.

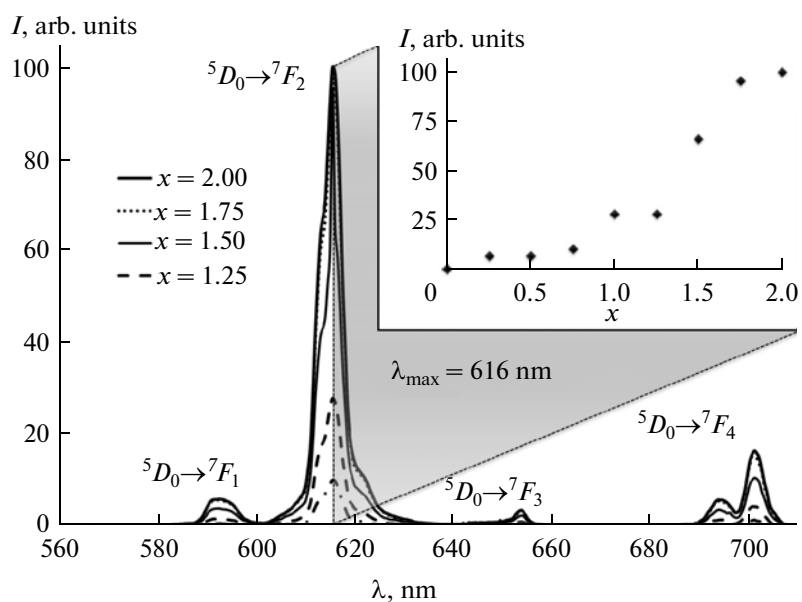


Fig. 7. Luminescence spectra ($\lambda_{\text{ex}} = 395$ nm) of α - $\text{Sm}_{2-x}\text{Eu}_x(\text{MoO}_4)_3$ and (inset) luminescence intensity in the range of the ${}^5D_0 \rightarrow {}^7F_2$ transition ($\lambda_{\text{max}} \sim 616$ nm) as a function of Eu^{3+} concentration.

decrease in luminescence intensity as the Eu^{3+} concentration in $\text{Sm}_{2-x}\text{Eu}_x(\text{MoO}_4)_3$ solid solutions increases from $x = 1.75$ to $x = 2$ is presumably caused by the concentration quenching effect. The absence of luminescence in the range of the ${}^5D_0 \rightarrow {}^7F_0$ transition (~ 580 nm) for all $\text{Sm}_{2-x}\text{Eu}_x(\text{MoO}_4)_3$ solid solutions is evidence of rather high symmetry of the oxygen environment of the Eu^{3+} cation.

As follows from Fig. 10, at $\lambda_{\text{ex}} = 395$ nm, the structure type has nearly no effect on the luminescence intensity of $\text{Sm}_{2-x}\text{Eu}_x(\text{MoO}_4)_3$ solid solutions in the range of the ${}^5D_0 \rightarrow {}^7F_2$ transition (the luminescence intensity in the range of the ${}^5D_0 \rightarrow {}^7F_2$ transition for α - and β' - $\text{Sm}_{2-x}\text{Eu}_x(\text{MoO}_4)_3$ modifications is actually the same). At the same time, the change in the excitation wavelength λ_{ex} 395 to 270 nm for the orthorhombic

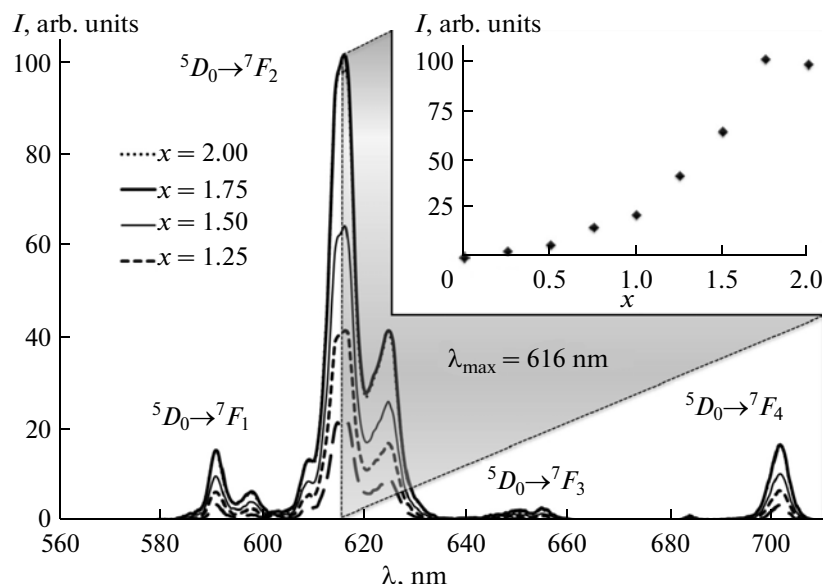


Fig. 8. Luminescence spectra of β' - $\text{Sm}_{2-x}\text{Eu}_x(\text{MoO}_4)_3$ at $\lambda_{\text{ex}} = 395$ nm and (inset) luminescence intensity in the range of the ${}^5D_0 \rightarrow {}^7F_2$ transition ($\lambda_{\text{max}} \sim 616$ nm) as a function of Eu^{3+} concentration.

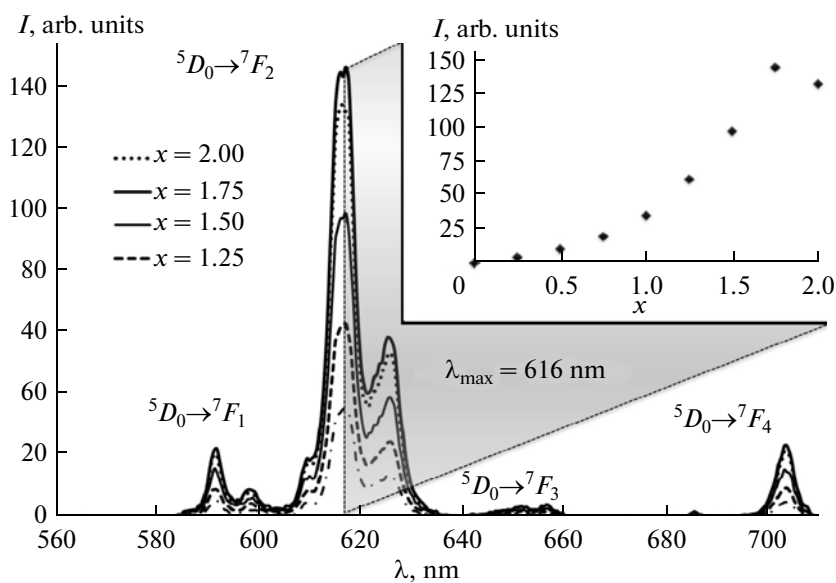


Fig. 9. Luminescence spectra of β' - $\text{Sm}_{2-x}\text{Eu}_x(\text{MoO}_4)_3$ at $\lambda_{\text{ex}} = 270$ nm and (inset) luminescence intensity in the range of the ${}^5D_0 \rightarrow {}^7F_2$ transition ($\lambda_{\text{max}} \sim 616$ nm) as a function of Eu^{3+} concentration.

β' - $\text{Sm}_{2-x}\text{Eu}_x(\text{MoO}_4)_3$ modifications leads to a significant increase in luminescence intensity of these solid solutions. For example, for β' - $\text{Sm}_{0.25}\text{Eu}_{1.75}(\text{MoO}_4)_3$, the luminescence intensity in the range of the ${}^5D_0 \rightarrow {}^7F_2$ transition increases by a factor of ~ 1.5 . Thus, the revealed change in the luminescence intensity in the range of the ${}^5D_0 \rightarrow {}^7F_2$ transition for β' - $\text{Sm}_{2-x}\text{Eu}_x(\text{MoO}_4)_3$ with a change of λ_{ex} from 395 to 270 nm shows that, for the β'

modifications, the luminescence excitation mechanism involving charge transfer to luminescent centers (Eu^{3+}) is more efficient than direct excitation of luminescent centers, as is the case for the monoclinic α phases.

Thus, $\text{Sm}_{2-x}\text{Eu}_x(\text{MoO}_4)_3$ solid solutions ($0 \leq x \leq 2$) in two modifications have been synthesized by a

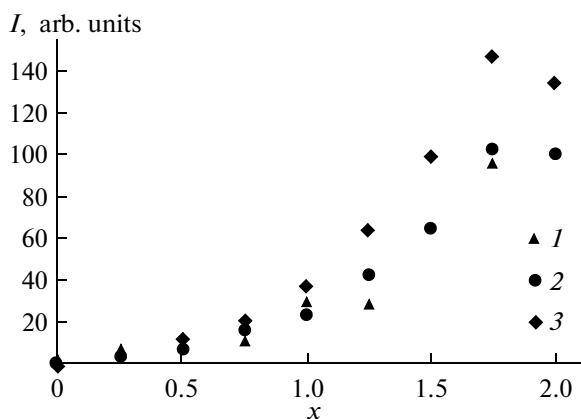


Fig. 10. Concentration dependence of luminescence intensity of the ${}^5D_0 \rightarrow {}^7F_2$ transition ($\lambda_{\max} \sim 616$ nm) for (1) α - $\text{Sm}_{2-x}\text{Eu}_x(\text{MoO}_4)_3$ and (2, 3) β' - $\text{Sm}_{2-x}\text{Eu}_x(\text{MoO}_4)_3$ at $\lambda_{\text{ex}} =$ (2) 395 and (3) 270 nm.

ceramic method: monoclinic α modification with a distorted scheelite structure (space group $C2/c$) and orthorhombic β' modification with a non-scheelite structure (space group $Pba2$). It has been found that the reversible first-order phase transition $\alpha \leftrightarrow \beta'$ for all $\text{Sm}_{2-x}\text{Eu}_x(\text{MoO}_4)_3$ solid solutions is accompanied by a significant increase in the unit cell volume ($\sim 24\%$). Studying the luminescence characteristics has shown that, for all $\text{Sm}_{2-x}\text{Eu}_x(\text{MoO}_4)_3$ solid solutions ($0 \leq x \leq 2$) irrespective of the structure type, the strongest intensity is inherent in the ${}^5D_0 \rightarrow {}^7F_2$ transition of the Eu^{3+} cation, which is responsible for the characteristic red luminescence of the samples ($\lambda_{\max} \sim 616$ nm). It has been elucidated that two luminescence excitation mechanisms have different contributions depending on the structure type: (1) direct excitation of Eu^{3+} cations (for the α modifications) and (2) excitation of luminescence centers through charge transfer from O^{2-} of in MoO_4^{2-} groups to the luminescent centers through the Mo–O bonds (for β' modifications). The luminescence intensity maximum for $\text{Sm}_{2-x}\text{Eu}_x(\text{MoO}_4)_3$ solid solutions, irrespective of the structure, is observed in the concentration range $1.75 \leq x \leq 2$.

ACKNOWLEDGMENTS

This work was supported by the Russian foundation for Basic Research (project nos. 14-03-01100 and 12-03-00124).

REFERENCES

1. V. K. Trunov, V. A. Efremov, and Yu. A. Velikodnyi, *Crystal Chemistry and Properties of Double Molybdates and Tungstates* (Nauka, Leningrad, 1986) [in Russian].
2. S. Neeraj, N. Kijima, and A. K. Cheetham, *Chem. Phys. Lett.* **387**, 2 (2004).

3. Q. Zeng, P. He, H. Liang, et al., *Mat. Chem. Phys.* **118**, 76 (2009).
4. A. Xie, X. Yuan, F. Wang, et al., *J. Alloys. Compd* **501**, 124 (2010).
5. L. Li, J. Zhang, W. Zi, et al., *Solid State Sci.* **29**, 58 (2014).
6. P. S. Dutta and A. Khanna, *ECS J. Solid State Sci. Technol.* **2**, R3153 (2013).
7. X. J. Geng, Y. W. Tian, Y. J. Chen, et al., *Appl. Phys.* **107**, 177.
8. N. C. George, K. A. Denault, and R. Seshadri, *Ann. Rev. Mater. Res.* **43**, 481 (2013).
9. F. B. Cao, L. S. Li, Y. W. Tian, et al., *Thin Solid Films* **519**, 7971 (2011).
10. Z. Wang, H. Liang, L. Zhou, et al., *Chem. Phys. Lett.* **412**, 313 (2005).
11. X. Zhao, X. Wang, B. Chen, et al., *Opt. Mater.* **29**, 1680 (2007).
12. X. He, M. Guan, Z. Li, et al., *J. Rare Earths* **28**, 878 (2010).
13. Y.-L. Yang, X.-M. Li, W.-L. Feng, et al., *J. Alloys Compd.* **505**, 239 (2010).
14. X. Zhao, X. Wang, B. Chen, et al., *J. Alloys. Compd.* **433**, 352 (2007).
15. X. Zhou, X. Yang, T. Xiao, et al., *J. Rare Earths* **31**, 655 (2013).
16. X. Liu, W. Xiang, F. Chen, et al., *Mater. Res. Bull.* **48**, 281 (2013).
17. Y. Deng, S. Yi, Y. Wang, et al., *Opt. Mater.* **36**, 1378 (2014).
18. H. J. Nassau, H. J. Levinstein, and G. M. Loiacono, *J. Phys. Chem. Solids* **26**, 1805 (1965).
19. P. B. Jamieson, S. C. Abrahams, and J. L. Bernstein, *J. Appl. Crystallogr.* **2**, 24 (1969).
20. T. Schustereit, S. L. Mueller, T. Schleid, et al., *Crystals* **1**, 244 (2011).
21. W. Jeitschko, *Acta Crystallogr., Sect. B: Struct. Sci.* **29**, 2074 (1973).
22. L. H. Brixner, P. E. Bierstedt, A. W. Sleight, et al., *Mater. Res. Bull.* **6**, 545 (1971).
23. J. Martinez-Garcia, A. Arakcheeva, P. Pattison, et al., *Phil. Mag. Lett.* **89**, 257 (2009).
24. I. Z. Hartenbach, *Anorg. Allg. Chem.* **634**, 2044 (2008).
25. D. Logvinovich, A. Arakcheeva, P. Pattison, et al., *Inorg. Chem.* **49**, 1587 (2010).
26. E. T. Keve, S. C. Abrahams, and J. L. Bernstein, *J. Chem. Phys.* **54**, 3185 (1971).
27. W. Jeitschko, *Acta Crystallogr., Sect. B* **28**, 60 (1972).
28. B. A. Marinkovic, P. M. Jardim, R. R. de Avillez, et al., *Solid State Sci.* **7**, 1377 (2005).
29. S. D. Gates and C. Lind, *J. Solid State Chem.* **180**, 3510 (2007).
30. X. -X. Wang, Y. -L. Xian, G. Wang, et al., *Opt. Mater.* **30**, 521 (2007).
31. R. D. Shannon, *Acta Crystallogr., Sect. A* **32**, 751 (1976).
32. S. -F. Wang, K. K. Rao, Y. -R. Wang, et al., *J. Am. Ceram. Soc.* **92**, 1732 (2009).
33. Y. Tian, X. Qi, X. Wu, et al., *Phys. Chem.* **113**, 10767.

Translated by G. Kirakosyan